

Numerical Simulation of Hydrodynamic Forces on a Submerged Floating Tunnel with Surface Roughness Subject to Wave Loading

Zou, Pengxu; Ruiter, Niels; Bricker, Jeremy D.; Uijtewaal, Wim S.J.

DOI

[10.17736/ijope.2024.ts27](https://doi.org/10.17736/ijope.2024.ts27)

Publication date

2024

Document Version

Final published version

Published in

International Journal of Offshore and Polar Engineering

Citation (APA)

Zou, P., Ruiter, N., Bricker, J. D., & Uijtewaal, W. S. J. (2024). Numerical Simulation of Hydrodynamic Forces on a Submerged Floating Tunnel with Surface Roughness Subject to Wave Loading. *International Journal of Offshore and Polar Engineering*, 34(2), 158–163. Article ISOPE-24-34-2-158. <https://doi.org/10.17736/ijope.2024.ts27>

Important note

To cite this publication, please use the final published version (if applicable). Please check the document version above.

Copyright

Other than for strictly personal use, it is not permitted to download, forward or distribute the text or part of it, without the consent of the author(s) and/or copyright holder(s), unless the work is under an open content license such as Creative Commons.

Takedown policy

Please contact us and provide details if you believe this document breaches copyrights. We will remove access to the work immediately and investigate your claim.

Numerical Simulation of Hydrodynamic Forces on a Submerged Floating Tunnel with Surface Roughness Subject to Wave Loading

Pengxu Zou*

CCCC Guangdong-Hong Kong-Macao Greater Bay Area Innovation Research Institute Ltd.
Zhuhai, China

Niels Ruiter

Department of Hydraulic Engineering, Delft University of Technology
Delft, The Netherlands

Jeremy D. Bricker

Department of Civil & Environmental Engineering, University of Michigan
Ann Arbor, Michigan, United States

Wim S. J. Uijtewaal

Department of Hydraulic Engineering, Delft University of Technology
Delft, The Netherlands

Marine biofouling is a major concern in the operational performance of submerged floating tunnels (SFTs). The objective of this research is to extend hydrodynamic conditions in experiments and numerically investigate the effects of marine fouling on the hydrodynamic behavior of SFTs, including flow characteristics and forces on the SFT subject to waves. A sensitivity analysis of roughness parameters including different roughness heights and roughness coverage ratios is carried out. Additionally, the hydrodynamic forces of a roughened SFT with a circular shape and a newly designed parametric shape are compared.

INTRODUCTION

For wide and deep-sea crossings, the submerged floating tunnel (SFT) is one of the alternatives to underwater tunnels and sea bridges. An SFT will, however, become colonized by marine species in a matter of weeks to years after installation, which then becomes one of the major challenges to the SFT's operating performance (Zou, Ruiter, Uijtewaal, et al., 2023).

The interaction between waves and marine-fouled structures is complex. Marine biofouling can create turbulence, eddies, and vortices that alter the way waves interact with the structure. This, in turn, can impact hydrodynamic forces that affect the stability and serviceability of structures. The marine fouling effects on the hydrodynamic forces on an SFT are first analyzed by the authors. The pressure distribution along the SFT, flow separation, and wake characteristics are numerally examined with respect to roughness parameters under steady currents (Zou, Ruiter, Bricker, and Uijtewaal, 2023). Furthermore, an experimental study of surface roughness effects on the dynamic response of an SFT has been performed at the Water Lab of Delft University of Technology (TU Delft), and the hydrodynamic forces on the SFT subject to currents, waves, and combined current-wave flows are evaluated (Zou, Ruiter, Uijtewaal, et al., 2023). However, because of

the limited experimental test conditions, the Keulegan-Carpenter number (KC) is rather low in the experiments. The effects of wave properties in a wider range of KC should be investigated as a further extension to the prior studies. In addition, the wake topology and vortex shedding characteristics of the SFT under waves should be further discussed, which were not properly measured in the experiments. Therefore, the current research deals with the effects of marine fouling on the hydrodynamic behavior of SFTs under waves.

Recent years have seen research on the impact of surface roughness on marine structures exposed to waves. The colonial hydroid *Ectopleura larynx* with different fouling lengths were tested under deep-water regular waves (Nobakht-Kolur et al., 2021). Realistic mussel roughness models featuring a variety of patterns and shapes were applied to investigate the hydrodynamics of horizontal cylinders subjected to oscillating flows (Marty et al., 2021). A set of experiments in a deep tank was conducted to study the effects of roughness height, roughness coverage ratio, and roughness type (gravel, mussels, kelp) on the fluid loading of offshore structures (Theophanatos and Wolfram, 1989). However, the effects of marine fouling on the wave-induced forces on an SFT have not received due attention. Prior research has focused on cross sections with simpler shapes (such as circles and rectangles), but no form comparison or optimization with regard to surface roughness has yet been done. A parametric shape proposed by Zou et al. (2020, 2021) was applied to an SFT to improve its hydrodynamic performance. Therefore, in this study, the hydrodynamic forces on SFTs with different cross sections—namely, circular and the parametric shapes—subject to wave loading are compared and evaluated.

For hydrodynamic force investigation, waves are frequently represented by planar oscillatory flows (Konstantinidis and Bouris,

*ISOPE Member.

Received August 11, 2023; updated and further revised manuscript received by the editors December 29, 2023. The original version (prior to the final updated and revised manuscript) was presented at the Thirty-third International Ocean and Polar Engineering Conference (ISOPE-2023), Ottawa, Canada, June 18–23, 2023.

KEY WORDS: Marine fouling, hydrodynamic forces, Morison equation, waves, roughness parameters, submerged floating tunnel, OpenFOAM.

2017; Pearcey et al., 2017). Kinematically, the horizontal component of the orbital velocity of waves can be represented by an oscillating planar flow, but dynamically, there is a difference. The hydrodynamic mass force is present, but the Froude-Krylov force of the inertia related to the absolute flow acceleration is not included. Therefore, the pressure gradient and boundary layer formation on the cylinder deviate from those of realistic waves. As a result of the variation in the force mechanism, the Morison equation's weighting of the drag and inertia components is erroneous. Furthermore, for horizontal cylinders as SFTs, the hydrodynamic forces are significantly affected by the vertical component of the orbital motion of the water particle (Teng, 1983). The planar oscillatory flow model neglects the free surface effects and vertical components of the water particle velocity, so it can overpredict the drag and inertia coefficients (Sarpkaya and Isaacson, 1981).

Therefore, to address the aforementioned questions, the effects of surface roughness on the hydrodynamic forces on SFTs under waves are experimentally and numerically investigated in this study. The hydrodynamic forces on SFT models with varying roughness heights and coverage ratios (CRs) are measured under regular waves. Furthermore, two types of SFT cross-sectional shapes (i.e., a parametric shape and a circular shape) have been tested to investigate the surface roughness effects for each cross-section shape.

METHODOLOGY

Experimental Setup

Physical model tests were conducted in a wave-current flume at the Water Lab of the Delft University of Technology. The flume has a length of 39 m, a width of 0.795 m, and a height of 1 m. To generate the desired incident waves, an automatic reflection compensation (ARC) system is used with a piston-type second-order wave generator with a maximum stroke length of 2 m. A passive wave absorber is positioned inside the flume end to prevent wave reflection. The heights of bare SFTs (without roughness elements) with the parametric and circular cross-section shapes are equal (0.16 m). To differentiate between reflected and incident waves, three wave gauges are positioned both ahead of and behind the SFT. The water level is 0.70 m. At 0.35 m below the free surface, two electromagnetic velocity meters of the Deltares E30 EMS probe type are deployed. The measurement of hydrodynamic force employs an ME (K3D60a) three-axis load cell boasting a ± 100 N load range and an accuracy of 0.5% relative to its full-scale range. Notably, this load cell has the capability to simultaneously quantify both horizontal and vertical forces exerted on the SFT. Data sampling is conducted at a frequency of 200 Hz, utilizing a block size consisting of two data points (Zou, Ruiter, Uijtewaal, et al., 2023). The experimental setups are shown in Fig. 1.

Numerical Setup

In the framework of the open source computational fluid dynamics toolbox OpenFOAM version 2006 (<http://www.openfoam.com>, last accessed date January 12, 2023), the impact of marine fouling represented by surface roughness on an SFT under waves is reproduced. The hydrodynamic forces of the SFT models with different roughness heights, roughness coverage ratios, and cross-section shapes are computed and compared.

Computational Domain. The computational domain has a length of 27 m and a height of 1.0 m. The water depth is 0.7 m. The center of the SFT is located 6 m from the inlet, with an internal flow blockage height (smooth SFT) of 16 cm.

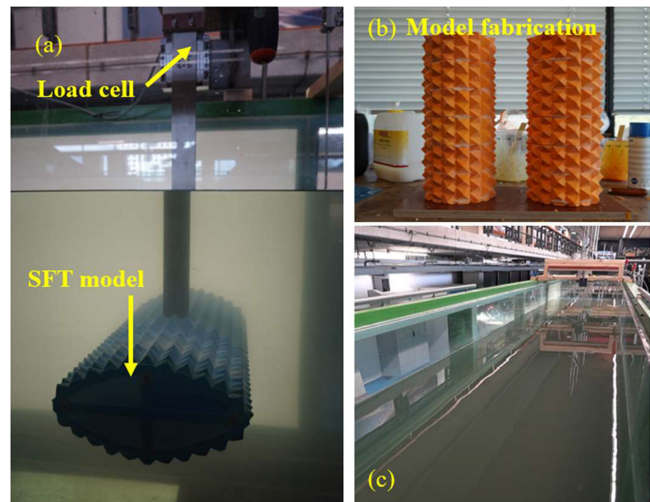


Fig. 1 (a) Experimental apparatus: Load cell attached to the SFT model, suspended from a stainless steel frame; (b) SFT model fabrication with circular shape and pyramidal roughness; and (c) wave-current flume used for the experiments

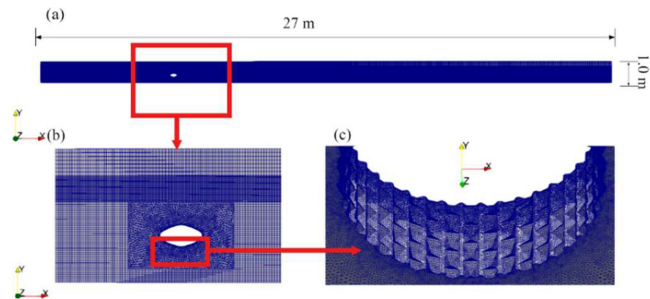


Fig. 2 Mesh configuration of the parametric shape SFT: (a) Computational domain of the numerical model, (b) mesh detail near the SFT, and (c) mesh detail of roughness elements

The transverse width of the numerical domain is 9 cm, including 3 or 6 roughness patterns in the spanwise direction for a roughness height of 1.5 cm or 0.5 cm, respectively. The side planes are symmetrically truncated with free-slip side boundaries.

In Fig. 2, the typical grid layout is displayed. The wave velocity is specified at the inlet, and an outflow boundary is employed at the outlet. On the SFT cross-section surface and at the bottom boundary, a no-slip wall condition is applied. For pressure reference, a pressure inlet is employed at the upper boundary. The first grid layer cell thickness normal to the SFT surface is within the acceptable range for y^+ of 30~200 (Kuzmin et al., 2007). The subdomain within the wave propagation region has horizontal and vertical mesh sizes of 0.2 cm and 2 cm, respectively. The cell size in the rest of the domain is 2 cm. The total number of cells ranges from 0.6 million up to 1.2 million, depending on the SFT model and roughness characteristics.

The unsteady Reynolds-averaged Navier-Stokes equations with an RNG k - ϵ turbulence model are applied with a standard wall function. The transient solver interFoam supplied with OpenFOAM for two-phase incompressible, isothermal immiscible fluids is applied. Nonlinear regular waves are generated using the second-order Stokes wave theory (Fenton, 1985) at the inlet open channel wave boundary. The phase-fraction-based interface capturing approach method (Hirt and Nichols, 1981) is applied to capture the wave surface. The pressure-velocity coupling and cor-

rection problem is solved using the combined PISO-SIMPLE algorithm. The upper limit for the Courant number is 0.5. An adaptive time step based on the Courant number was applied after the initial time step of 0.01 s.

Turbulence Model. With the inclusion of an additional term to its equation, the renormalization group (RNG) k - ε model is more accurate and robust than the traditional k - ε model for a wider class of flows (Zou et al., 2020). Therefore, the RNG k - ε model is applied in the SFT-wave simulation. The energy and dissipation equations for the RNG k - ε model are given by

$$\begin{aligned} & \frac{\partial}{\partial t}(\rho k) + \frac{\partial}{\partial x_i}(\rho k u_i) \\ &= \frac{\partial}{\partial x_j} \left(\alpha_k \mu_{\text{eff}} \frac{\partial k}{\partial x_j} \right) + G_k + G_b - \rho \varepsilon - Y_M + S_k \\ & \frac{\partial}{\partial t}(\rho \varepsilon) + \frac{\partial}{\partial x_i}(\rho \varepsilon u_i) \\ &= \frac{\partial}{\partial x_j} \left(\alpha_\varepsilon \mu_{\text{eff}} \frac{\partial \varepsilon}{\partial x_j} \right) + C_{1\varepsilon} \frac{\varepsilon}{k} (G_k + C_{3\varepsilon} G_b) - C_{2\varepsilon} \rho \frac{\varepsilon^2}{k} \\ & \quad + G_b - R_\varepsilon + S_\varepsilon \end{aligned} \quad (1)$$

where $C_1 = 1.42$, $C_2 = 1.68$, μ_{eff} is the effective viscosity, ρ is the fluid density, G_k and G_b are turbulence generation terms, Y_m is the contribution of the fluctuating dilatation of compressible turbulence to the overall dissipation rate, S_k and S_ε are source terms, k is turbulence kinetic energy, and ε is the turbulence dissipation rate.

The additional term in the ε equation is given by

$$R_\varepsilon = \frac{C_\mu \rho \eta^3 (1 - \eta/\eta_0) \varepsilon^2}{1 + \beta \eta^3} \frac{\varepsilon^2}{k} \quad (2)$$

where $\eta \equiv S_k/\varepsilon$, $\eta_0 = 4.38$, and $\beta = 0.012$.

The turbulent viscosity can be computed by

$$\mu_t = \rho C_\mu \frac{k^2}{\varepsilon} \quad (3)$$

where $C_\mu = 0.085$.

Test Cases

Under various regular wave conditions, the effects of SFT cross-section shape, roughness height (K), and fouling coverage ratio (CR) on the hydrodynamic forces on an SFT are compared and studied. For the SFT models, two cross-section shapes (i.e., circular and parametric shapes) are tested. For the roughness elements, a staggered pattern is designed to prevent sheltering effects, and a pyramidal roughness pattern is applied to lessen uncertainty related to the intricate biological processes. Two roughness heights are chosen (i.e., 15 mm and 5 mm), and two roughness coverage ratios including 100% and 50% are included to investigate the three-dimensional impacts of surface roughness. The characteristics of the SFT models are listed in Table 1. The definitions of k_s , D_{ex} , and D_{ez} can be found in the following section.

The generated wave has a height of up to 0.16 m and a wave period of up to 1.84 s in the laboratory flume experiments (W1~W5; see Table 2). The wave conditions in the experiments have been extended in the numerical model to determine the relationship between the drag and inertia coefficients of the SFT and the hydrodynamic metrics across a wider range (bigger KC). Therefore, the SFT under waves W6~W8 are simulated in the numerical models. The test conditions are listed in Table 2. The wave steepness is defined as the ratio of wave height to wave length.

Model	Cross section	K (cm)	CR (%)	k_s (cm)	D_{ex} (m)	D_{ez} (m)
1	Circular	1.5	100	0.75	0.175	0.175
2	Parametric	1.5	100	0.75	0.175	0.335
3	Parametric	1.5	50	0.375	0.1675	0.3275
4	Parametric	0.5	100	0.25	0.165	0.325

Table 1 Main characteristics of the modeled SFT

Environment	Label	Wave height (m)	Wave period (s)	Wave steepness (—)
Wave	W1	0.08	1.12	0.042
	W2	0.08	1.41	0.028
	W3	0.08	1.84	0.019
	W4	0.12	1.84	0.029
	W5	0.16	1.84	0.039
	W6	0.16	2.50	0.026
	W7	0.16	3.50	0.018
	W8	0.16	4.50	0.014

Table 2 Environmental conditions used in the numerical models

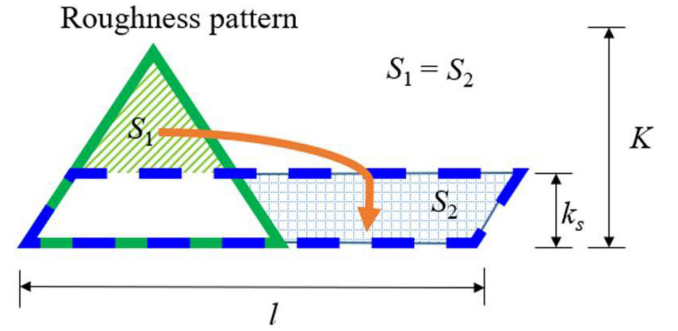


Fig. 3 Typical roughness patterns and reduced roughness height: k is the actual roughness height, l is the length of the repetitive roughness patterns, and S_1 and S_2 are the areas of the marked region.

Performance Metrics

Because there is no universal roughness function that applies to all types of roughness, an equivalent diameter considering roughness parameters is proposed (Zou, Ruiter, Uijtewaal, et al., 2023). The equivalent diameter determined by an equivalent blockage area is given by

$$D_{ei} = D_i + 2k_s \quad (4)$$

where D_i is the bare SFT dimension; $i, j = x, z$ represents the horizontal and vertical directions, respectively. k_s is the reduced roughness height with an equal blockage area.

The objective is to find a quadrangle with the same blockage cross-sectional area as the original repetitive roughness elements, shown in Fig. 3 (Zou, Ruiter, Uijtewaal, et al., 2023).

Wave forces and related dimensionless coefficients can be used to quantify how surface roughness affects the hydrodynamic characteristics of an SFT. Based on the Morison equation, the wave force acting on the SFT is given by

$$\begin{aligned} F &= F_d + F_m + F_p = \frac{1}{2} \rho C_d D_e U |U| + \rho C_A A_e \dot{U} + \rho A_e \ddot{U} \\ &= \frac{1}{2} \rho C_d D_e U |U| + \rho C_m A_e \dot{U} \end{aligned} \quad (5)$$

where U is the wave orbital velocity; C_d is the mean drag coefficient; F_d is the time-averaged drag force per unit of length; D_e denotes the equivalent diameter of the SFT; ρ is fluid density; F_m and F_p stand for the hydrodynamic-mass force and the Froude-Krylov force, respectively; A_e is the SFT's equivalent cross-sectional area when surface roughness is taken into account; \dot{U} is water particle acceleration; C_A is the hydrodynamic-mass coefficient; and $C_m = C_A + 1$, which is the inertia coefficient.

For horizontal cylinders such as SFTs, the Morison equation should be modified, assigned as two force coefficients in the horizontal and vertical directions, respectively (Chaplin, 1988). The hydrodynamic forces acting on the SFT are therefore described by the modified Morison equation, given by

$$F_i = \frac{1}{2} \rho C_{di} D_{ej} U_i \sqrt{U_x^2 + U_z^2} + \rho C_{mi} A_e \dot{U}_i \quad (6)$$

where F_i represents the wave force on the SFT per unit length. The drag and inertia coefficients were calculated by the least squares method, which solves the system of Eqs. 7~10, given by

$$f_{di} \sum [U_i^2 (U_x^2 + U_z^2)] + f_{mi} \sum (U_i \sqrt{U_x^2 + U_z^2} \dot{U}_i) = F_{di} \sum (U_i \sqrt{U_x^2 + U_z^2}) \quad (7)$$

$$f_{di} \sum [U_i \sqrt{U_x^2 + U_z^2} \dot{U}_i] + f_{mi} \sum (\dot{U}_i^2) = F_{di} \sum \dot{U}_i \quad (8)$$

$$f_{di} = \frac{1}{2} \rho C_{di} D_{ej} \quad (9)$$

$$f_{mi} = \rho C_{mi} A_e \quad (10)$$

where F_i is the force per unit length on the SFT. The KC is a critical parameter that is utilized and described as follows when examining hydrodynamic features and flow properties:

$$KC_i = \frac{U_{mi} T}{D_{ei}} \quad (11)$$

where U_m is the maximum orbital velocity of waves at the half water depth (same depth as the SFT); T is the wave period.

MODEL VALIDATION

The numerical results for the drag and inertia coefficients for the SFT with a roughness height of 1.5 cm for the circular and parametric cross-section shapes (Models 1 and 2) are plotted against KC and compared with experimental data (with error bars) in Fig. 4.

Figure 4 shows a reasonable agreement, implying the validity of the numerical results. Note that the $C_{d,z}$ of the circular SFTs can take negative values in the experiments (Fig. 4b). This is likely because the vertical drag force component is rather small at low KC values; the $C_{d,z}$ computation is therefore highly sensitive to the time shift of the measured force signals (between the location of velocity measurement and the location of force measurement), and thus generates a large error.

RESULTS

Effects of Roughness Height and Coverage Ratio

To figure out the relationship of the drag and inertia coefficients of the SFT with the hydrodynamic conditions over a wider range (larger KC), the conditions in the experiments have been extended in the numerical model.

Figure 5 shows the drag and inertia coefficients of the three SFT configurations as a function of KC . It appears that both

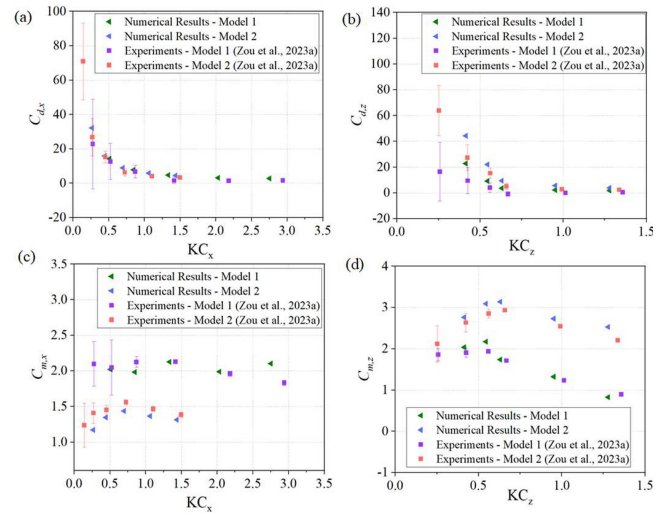


Fig. 4 Hydrodynamic force coefficient validation

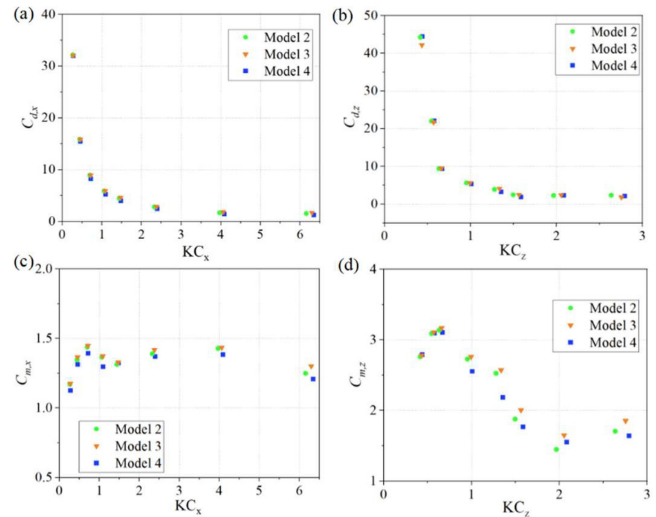


Fig. 5 Distribution of drag and inertia coefficients as a function of the Keulegan–Carpenter number KC (in the horizontal and vertical directions) for the SFT configurations: Model 2 (parametric shape with roughness height = 1.5 cm), Model 3 (parametric shape with roughness coverage ratio = 50%), and Model 4 (parametric shape with roughness height = 0.5 cm) under wave forcing

$C_{d,x}$ and $C_{d,z}$ increase exponentially with decreasing KC for the three configurations (Fig. 5, panels a and b). The three configurations do not significantly differ in $C_{d,x}$ and $C_{d,z}$, proving that the roughness height and coverage ratio are not crucial parameters for $C_{d,x}$ and $C_{d,z}$ in wave conditions. Panels c and d of Fig. 5 show that Model 4 (parametric $K = 0.5$ cm) generally has the lowest $C_{m,x}$ and $C_{m,z}$ values, and Model 4 (parametric $CR = 50\%$) has slightly higher $C_{m,x}$ and $C_{m,z}$ values than Model 2 (parametric $K = 1.5$ cm). For all parametric shape configurations, with increasing KC , $C_{m,x}$ exhibits an abrupt increase, leveling off at $KC = 1$, whereas $C_{m,z}$ shows an increase followed by a decline with a minimum at $KC = 2$.

Effects of Cross-section Shape

The hydrodynamic force coefficients of the circular and parametric shapes are displayed in Fig. 6. The hydrodynamic force coefficients in the horizontal and vertical directions are shown as

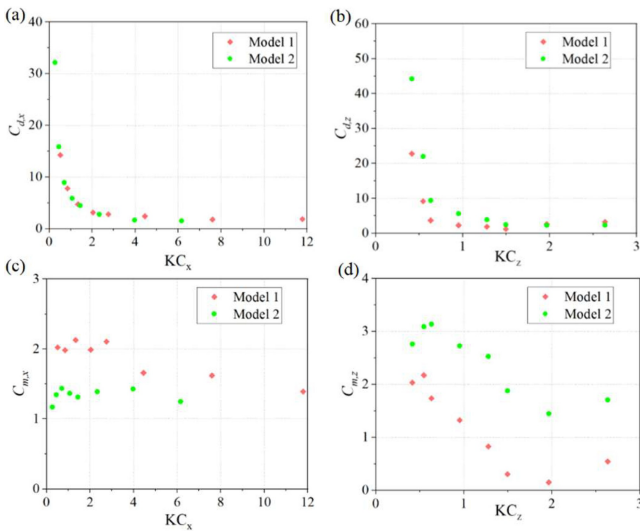


Fig. 6 Distribution of drag and inertia coefficients as a function of the Keulegan-Carpenter number KC (in the horizontal and vertical directions) for the SFT configurations: Model 1 (circular shape with roughness height = 1.5 cm) and Model 2 (parametric shape with roughness height = 1.5 cm) under wave forcing

a function of KC . It should be noted that the parametric shape has a larger horizontal dimension than the circular shape, which results in a smaller KC_x value for the parametric shape under identical wave conditions. However, for an equal blockage height, KC_z is the same for the two cross-section shapes (Fig. 6b). This shows that for all the configurations, the drag coefficients increase exponentially as KC decreases. The parametric shape has a larger C_d when $KC < 1.8$, whereas for $KC > 1.8$, the circular shape has a larger C_d . This can be attributed to the parametric shape's longer perimeter and greater quantity of surface roughness elements, which cause a larger frictional drag than the circular shape experiences. However, as KC increases, vortex shedding is generated, in which case the form drag plays a more important role in the total drag. The parametric shape has a more streamlined shape, which can reduce the C_d when form drag dominates. With increasing KC_z , the $C_{d,z}$ of both shapes declines abruptly at about $KC_z = 0.6$ before leveling off, and a gradual increase of $C_{d,z}$ can be observed when KC_z further increases.

Shown in Fig. 6c is the $C_{m,x}$ of the rough SFTs with both circular and parametric cross sections. The parametric-shaped SFT has a significantly lower $C_{m,x}$ than the circular shape. The circular shape exhibits a generally constant $C_{m,x}$ when $KC_x < 3$, followed by a marked reduction and a further minor decrease in inertia coefficients with increasing KC , whereas for the parametric shape, the variation of $C_{m,x}$ with KC is not obvious. On the contrary, the horizontal cross-section area subject to vertical wave motion is larger for the parametric cross section than for the circular one. As a result, $C_{m,z}$ is larger for the parametric shape than the circular shape (Fig. 6d). Additionally, in contrast to the horizontal inertia coefficients, the vertical inertia coefficients drop more rapidly with increasing KC , followed by an increase, with a minimum value at $KC_z = 2$.

The vorticity around the SFT, calculated by the mean velocity field for circular and parametric cross-section shapes at different wave conditions, is depicted in Fig. 7. It demonstrates that for the W4 condition, the thickness of the strong vorticity region surrounding both shapes is low, and no localized vorticity can be seen, indicating that no vortex shedding occurs. For the W6 condition, the attached vortices around the circular shape disintegrate,

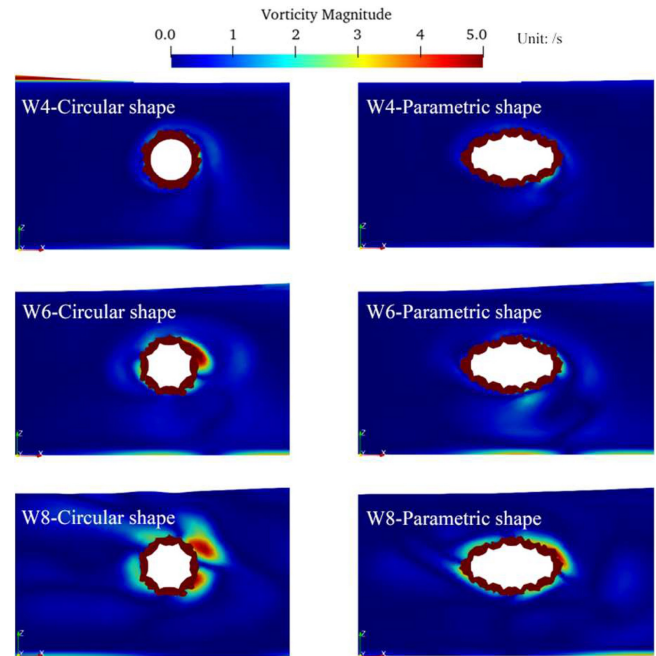


Fig. 7 Mean vorticity field around the SFT for circular and parametric shapes under different wave conditions

and asymmetric vortices at both leading and trailing edges are generated. Near the upper surface of the downstream side, strong vorticity exists. No significant vortices, however, occur behind the SFT for the parametric shape. For the W8 condition, both shapes form vortex pairs. It can be observed that vortices shed behind the SFT grow larger in size and higher in vorticity magnitude with the circular cross section compared with the parametric cross section. Because of the parametric shape's more streamlined shape, the vortex shedding is generated at a larger KC compared with the circular shape. It can be noted that with increasing KC , vortex shedding at both leading and trailing edges occurs, and the lift force is no longer nil. This flow regime has a nonzero mean lift because of asymmetry, and the direction of this lift force will shift in accordance with the side of the vortex street.

CONCLUSIONS

This paper presents a numerical study of marine fouling (represented by surface roughness) effects on the hydrodynamic forces and flow characteristics of an SFT under regular waves. The influence of cross-section shape and roughness parameters (i.e., roughness height and roughness coverage ratio) on the wave force coefficients of the SFT is assessed. The main findings are summarized as follows:

1. The roughness parameters including roughness height and coverage ratio have little effect on C_d and C_m for wave conditions.
2. The parametric shape has a much lower horizontal inertia coefficient than the circular shape. However, because of the longer horizontal dimension and larger cross-sectional area of the parametric shape, its vertical wave force coefficients are larger than those of the circular shape for a small KC .
3. Under the same wave conditions, the circular shape generates larger vortices and higher vorticity than the parametric shape. As KC increases, vortex shedding occurs, and a lift force is generated.

The study's findings contribute to a better understanding of the impact of marine fouling on the SFT's hydrodynamic performance in the presence of waves. The assessed results of the hydro-

dynamic force in relation to the factors of structural geometry and roughness can provide references for the engineering design of SFTs. It is important to highlight that this research primarily focuses on regular waves. However, it is essential to acknowledge the significance of examining the effects of surface roughness on significant wave height under irregular wave conditions, which warrants attention in future research endeavors.

ACKNOWLEDGEMENTS

The study presented in this paper was conducted in the submerged floating tunnel research project led by China Communications Construction Company Ltd. (CCCC). Funding for reporting was obtained from the Cooperative Institute for Great Lakes Research (CIGLR) postdoctoral fellowship.

REFERENCES

- Chaplin, JR (1988). "Loading on a Cylinder in Uniform Oscillatory Flow: Part I—Planar Oscillatory Flow," *Appl Ocean Res*, 10(3), 120–128. [https://doi.org/10.1016/S0141-1187\(88\)80012-9](https://doi.org/10.1016/S0141-1187(88)80012-9).
- Fenton, JD (1985). "A Fifth-order Stokes Theory for Steady Waves," *J Waterw Port Coastal Ocean Eng*, 111(2), 216–234. [https://doi.org/10.1061/\(ASCE\)0733-950X\(1985\)111:2\(216\)](https://doi.org/10.1061/(ASCE)0733-950X(1985)111:2(216)).
- Hirt, CW, and Nichols, BD (1981). "Volume of Fluid (VOF) Method for the Dynamics of Free Boundaries," *J Comput Phys*, 39(1), 201–225. [https://doi.org/10.1016/0021-9991\(81\)90145-5](https://doi.org/10.1016/0021-9991(81)90145-5).
- Konstantinidis, E, and Bouris, D (2017). "Drag and Inertia Coefficients for a Circular Cylinder in Steady plus Low-amplitude Oscillatory Flows," *Appl Ocean Res*, 65, 219–228. <https://doi.org/10.1016/j.apor.2017.04.010>.
- Kuzmin, D, Mierka, O, and Turek, S (2007). "On the Implementation of the $k-\varepsilon$ Turbulence Model in Incompressible Flow Solvers Based on a Finite Element Discretisation," *Int J Comput Sci Math*, 1(2/3/4), 193–206. <https://doi.org/10.1504/ijcsm.2007.016531>.
- Marty, A, et al. (2021). "Experimental Study of Hard Marine Growth Effect on the Hydrodynamical Behaviour of a Submarine Cable," *Appl Ocean Res*, 114, 102810. <https://doi.org/10.1016/j.apor.2021.102810>.
- Nobakht-Kolur, F, Zeinoddini, M, Harandi, MA, Abi, FA, and Jadidi, P (2021). "Effects of Soft Marine Fouling on Wave-induced Forces in Floating Aquaculture Cages: Physical Model Testing under Regular Waves," *Ocean Eng*, 238, 109759. <https://doi.org/10.1016/j.oceaneng.2021.109759>.
- Pearcey, T, Zhao, M, Xiang, Y, and Liu, M (2017). "Vibration of Two Elastically Mounted Cylinders of Different Diameters in Oscillatory Flow," *Appl Ocean Res*, 69, 173–190. <https://doi.org/10.1016/j.apor.2017.11.003>.
- Sarpkaya, T, and Isaacson, M (1981). *Mechanics of Wave Forces on Offshore Structures*, Van Nostrand Reinhold, 651 pp.
- Teng, C-C (1983). *Hydrodynamic Forces on a Horizontal Cylinder under Waves and Current*, Master's thesis, Oregon State University, Corvallis, OR, USA, 115 pp.
- Theophanatos, A, and Wolfram, J (1989). "Hydrodynamic Loading on Macro-Roughened Cylinders of Various Aspect Ratios," *J Offshore Mech Arct Eng*, 111(3), 214–222. <https://doi.org/10.1115/1.3257150>.
- Zou, P, Bricker, J, and Uijtewaal, W (2020). "Optimization of Submerged Floating Tunnel Cross Section Based on Parametric Bézier Curves and Hybrid Backpropagation—Genetic Algorithm," *Mar Struct*, 74, 102807. <https://doi.org/10.1016/j.marstruc.2020.102807>.
- Zou, P, Bricker, JD, and Uijtewaal, W (2021). "Submerged Floating Tunnel Cross-section Analysis Using a Transition Turbulence Model," *J Hydraul Res*, 60(2), 258–270. <https://doi.org/10.1080/00221686.2021.1944921>.
- Zou, P, Ruitter, N, Bricker, JD, and Uijtewaal, WSJ (2023). "Effects of Roughness on Hydrodynamic Characteristics of a Submerged Floating Tunnel Subject to Steady Currents," *Mar Struct*, 89, 103405. <https://doi.org/10.1016/j.marstruc.2023.103405>.
- Zou, P, Ruitter, N, Uijtewaal, WSJ, et al. (2023). "Experimental Study of Surface Roughness Effects on Hydrodynamic Characteristics of a Submerged Floating Tunnel," *Appl Ocean Res*, 135, 103557. <https://doi.org/10.1016/j.apor.2023.103557>.